Medical Engineering and Physics 46 (2017) 1–11

Contents lists available at ScienceDirect

Medical Engineering and Physics

journal homepage: www.elsevier.com/locate/medengphy

A custom-made temporomandibular joint prosthesis for fabrication by selective laser melting: Finite element analysis

Xiangliang Xu[a,1], Danmei Luo[b,1], Chuanbin Guo[a,*], Qiguo Rong[b,**]

[a] National Engineering Laboratory for Digital and Material Technology of Stomatology, Department of Oral and Maxillofacial Surgery, Peking University School and Hospital of Stomatology, Beijing, China
[b] Department of Mechanics and Engineering Science, College of Engineering, Peking University, Beijing, China

ARTICLE INFO

Article history:
Received 3 August 2016
Revised 28 February 2017
Accepted 13 April 2017

Keywords:
Temporomandibular joint
Joint prosthesis model
Biomechanics
Finite element analysis

ABSTRACT

A novel and custom-made selective laser melting (SLM) 3D-printed alloplastic temporomandibular joint (TMJ) prosthesis is proposed. The titanium-6aluminium-4vanadium (Ti-6Al-4V) condyle component and ultra-high molecular weight polyethylene (UHMWPE) fossa component comprised the total alloplastic TMJ replacement prosthesis. For the condyle component, an optimized tetrahedral open-porous scaffold with combined connection structures, i.e. an inlay rod and an onlay plate, between the prosthesis and remaining mandible was designed. The trajectory of movement of the intact condyle was assessed via kinematic analysis to facilitate the design of the fossa component. The behaviours of the intact mandible and mandible with the prosthesis were compared. The biomechanical behaviour was analysed by assessing the stress distribution on the prosthesis and strain distribution on the mandible. After muscle force was applied, the magnitude of the compressive strain on the condyle neck of the mandible with the prosthesis was lower than that on the condyle neck of the intact mandible, with the exception of the area about the screws; additionally, the magnitude of the strain at the scaffold–bone interface was relatively high.

1. Introduction

The temporomandibular joint (TMJ) plays a unique and crucial role in our daily life, as it is involved in speech, expression and chewing. TMJ defects are caused by trauma, infection, tumour, ankylosis, and/or idiopathic resorption. Reconstruction of acquired TMJ defects is an obvious challenge in oral and maxillofacial surgery. Several techniques have been developed over the decades, such as costochondral grafting, iliac crest bone grafting, distraction osteotomy, fibular free flap, and alloplastic TMJ implants [1,2]. As compared to autogenous reconstruction, an alloplastic TMJ prosthesis can reduce donor site morbidity, provide immediate function, and be customizable. Although all of the currently available alloplastic TMJ implants have shown promise, artificial TMJs have not been accepted as universally as artificial hip and knee joints, as these were introduced several decades ago [3,4]. In addition to the biocompatibility problems that caused severe implant failures in the early 1980s [5], another main reason for concern has been the highly complex biomechanical role of the TMJ.

The TMJ is the point of articulation for the mandible, articular discs, and the base of the skull, which connects at the left and right joints. In order to adapt to different vital functions, mandibular condyles with incongruent surfaces carry out extremely complex movements with respect to the base of skull [6,7]. Accordingly, researchers have recommended the use of custom-made TMJ prostheses rather than stock prostheses, as custom-made TMJs can be better fitted to the anatomical structures of each individual to ensure correct physiological functioning [1,8–10].

Additive manufacturing techniques have been used recently for the construction of customized artificial TMJs. According to some studies [3,8,11], these products could improve the outcomes of artificial TMJ restoration. However, the design of the artificial fossa of the TMJ does not permit it to guide the movement of the artificial condyle along its physiological trajectory; thus, deviation of mandibular movement can occur, with the healthy contralateral TMJ suffering a secondary injury [9,12,13]. Moreover, currently available TMJ implants are all made of internally homogenized metal; therefore, the stiffness of the artificial condyle is much higher than that of condylar cortical and trabecular bone, which could readily induce a stress shielding effect subsequent to long-term usage [14,15].

* Corresponding author.
** Corresponding author.
E-mail addresses: guodazuo@vip.sina.com (C. Guo), qrong@pku.edu.cn (Q. Rong).
[1] Xiangliang Xu and Danmei Luo contributed equally to this article.

http://dx.doi.org/10.1016/j.medengphy.2017.04.012
1350-4533/

Several additive manufacturing techniques have recently been developed to fabricate structures for tissue engineering [16]. Among these approaches, selective laser melting (SLM) has been confirmed to be able to fabricate objects with precise internal architecture and external profiles. Several studies have shown that additive manufacturing of titanium alloy scaffolds can be used to repair bone defects because it has similar biomechanical properties [17–19]. A few researchers designed and fabricated a customized pure titanium condyle via selective laser melting technology in 2014 [20]. They designed a hollow structure for the condyle component by using two titanium plates to fix the prosthesis onto the outer surface of remaining mandible, an approach of fabricating the internal structure and connection design of the condyle component that differs from that of the present study. Considering these results, this technique may be suitable for the fabrication of a novel TMJ prosthesis.

A canine model was used in this study, as it has two left and right temporomandibular articular complexes, each of which comprises a condylomeniscal and meniscotemporal joint on either side, similar to the structure in humans. Both canine and human TMJs have a condylar joint and a reciprocally fitting one. The masseter, temporalis, and pterygoid muscles supporting the condylar processes within the fossa in canines are similar to those in humans. Canines also perform open–close and lateral movements of the mandible, despite their comparatively small range of lateral movement [21,22]. Several studies have been conducted on the TMJ using canine models, including temporomandibular joint meniscus reconstruction and unilateral condylectomy [23,24]. The ultimate goal of our research is to design TMJ prosthesis for humans. In this initial study, we obtained individual trajectories of condyle movement in the canine model and applied this information in the subsequent design of the articular surface of the TMJ fossa component. In a human study, we would use this same procedure to obtain the lower surface of the fossa component. Although the movement of the canine mandible differs from that of humans, the method with which we collected the envelope surface of condyle movement trajectory would be similar. As with the animal experiment, we will test the hypothesis that the custom-made prosthesis design can endure individual TMJ movement variations. If similar in vivo findings are achieved, the same procedure will be used to design TMJ prosthesis for humans by first obtaining individual trajectories of TMJ movement, and then by designing the customized articular surface.

Finite element analysis (FEA) is well established in the study of the biomechanical behaviour of the TMJ [25–28]. In this study, the individually designed TMJ prosthesis was constructed and tested using FEA. To reduce the stress shielding effect, the trabecular design in the novel TMJ prosthesis was optimized to be comparable to the structural modulus of bone. An inlay rod and an onlay plate were designed to strengthen the connection between the prosthesis and the remaining bone. To maintain healthy movement of the mandibular condyle, the articular surface of the prosthetic fossa component was designed with specific consideration for condylar movement. The reliability of the prosthesis was demonstrated by comparing the behaviour of an intact mandible and a mandible with the customized TMJ prosthesis.

2. Materials and methods

2.1. Computer-aided design (CAD) models

The bone structure morphology of the TMJ was constructed to accommodate an adult beagle canine. Computed tomography (CT) scans were performed using an 8-slice scanner (BrightSpeed, GE Medical Systems, USA) with a rotation time of 1 s, a slice thickness of 1.25 mm, voltage between 120 and 140 kV, and automatic exposure control. CT images were taken for four positions of the mandible: closed, 1/3-open, 2/3-open, and widest open positions.

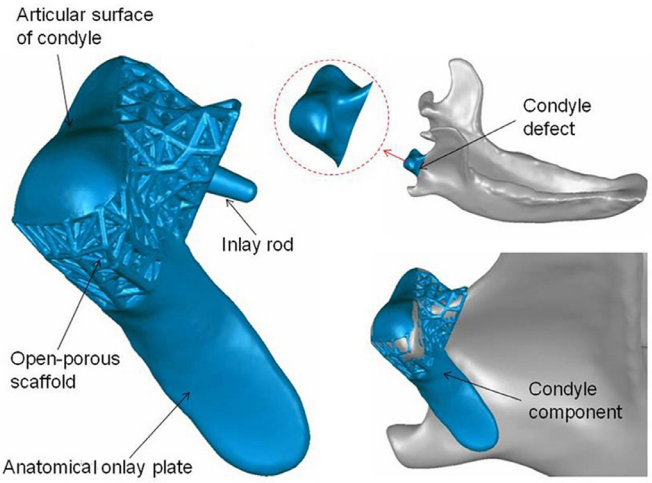

Fig. 1. Condyle component structure and design of the replacement prosthesis. Left panel: the profile of the condyle prosthesis; top right panel: the condyle defect region marked in blue in the intact mandible; lower right panel: the condyle defect region replaced by the condyle prosthesis. (For interpretation of the references to colour in this figure legend, the reader is referred to the web version of this article.)

2.2. Design of the custom-made TMJ prosthesis

The individually designed TMJ implant was a total TMJ replacement prosthesis composed of condyle and fossa components, which were fixed to the mandible and zygoma separately with three screws and four screws, respectively. The prosthesis was installed on the right side of the mandible. Because of clinical experience and knowledge of the anatomy of a beagle skull, four screws were chosen to fix the fossa component to the cranium, and three screws were used to fix the condyle to the mandible. The screws used for the TMJ fixation were 2.0 mm in diameter, which is considered the minimum diameter able to provide sufficient stability [29]. The condyle component comprised titanium-6aluminium-4vanadium alloy (Ti-6Al-4 V), which was created using the Mlab Cusing 3D Metal Printing Machine (Concept Laser, Lichtenfels, Germany). The accuracy of the machine was approximately 40 μm. The fossa component consisted of ultra-high molecular weight polyethylene (UHMWPE), which was manufactured using a computerized numerical control machine (Dima Digital Machine, Shenzhen, China). The screws were also Ti-6Al-4 V alloy.

2.2.1. Design of the condyle component

The defect region of the mandible in this study included the entire condyloid process spanning from the mandibular notch to the posterior border of the mandibular ramus (Fig. 1). The condyle component of the TMJ prosthesis was designed to restore the condyle defect. The condyle component was designed as shown in Fig. 1. The profile of the condyle component was based on the anatomical shape of the condyle of the beagle model. Atop the condyle component was a preserved layer of 1-mm-thick condyle articular surface with a polished outer surface. This 1-mm-thick layer played an important role in load bearing and load transmission between the fossa and condyle components during mastication. The polished articular surface was purposed to decrease friction ratio and material wear. This layer was modelled as a solid entity in the FEA model; the friction ratio between the interface of the fossa component and condyle component was set to be 0.01.

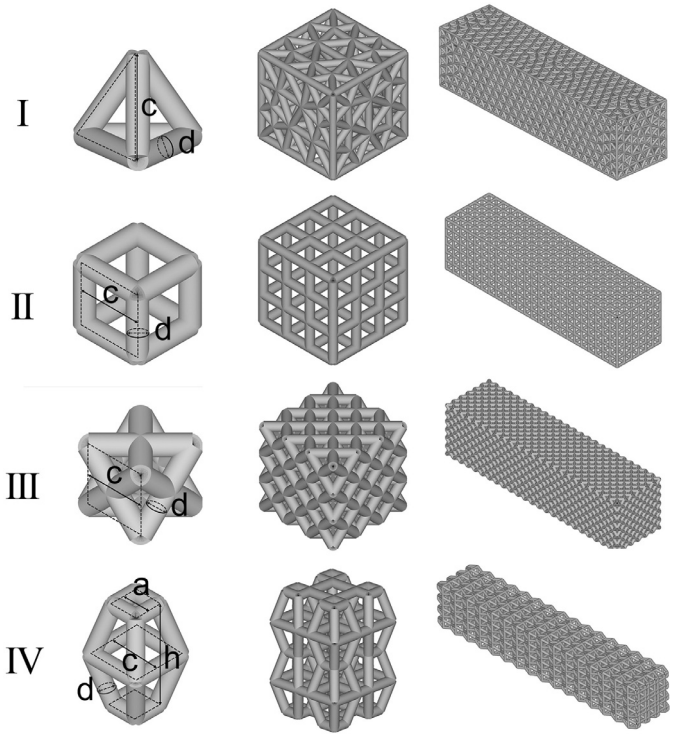

Fig. 2. Mechanically tested scaffolds of the tetrahedral, cubic, diagonal, and truncated pyramidal structures and their respective parameterized models with the size of the basic cell (c) and strut diameter (d). Rows I, II, III, and IV correspond to the parameterized structures and mechanically tested scaffolds of the tetrahedral structure, cubic structure, diagonal structure and truncated pyramidal structure, respectively. In each row, the structure is shown on the left, the compression-tested scaffold is shown in the middle, and the bending- and torsion-tested scaffold is shown on the right. In row IV, 'a' refers to the length of an additional connection strut and 'h' refers to the height of a basic cell. For rows I, II, and III, the side length of the compression-tested models was $3c \times 3c \times 3c$, and the side length of the bending- and torsion-tested models was $6c \times 6c \times 24c$. For row IV, the side length of the compression-tested model was $(2c+a) \times (2c+a) \times 2\,h$, and the side length of the bending- and torsion-tested models was $(4c+3a) \times (4c+3a) \times 16\,h$.

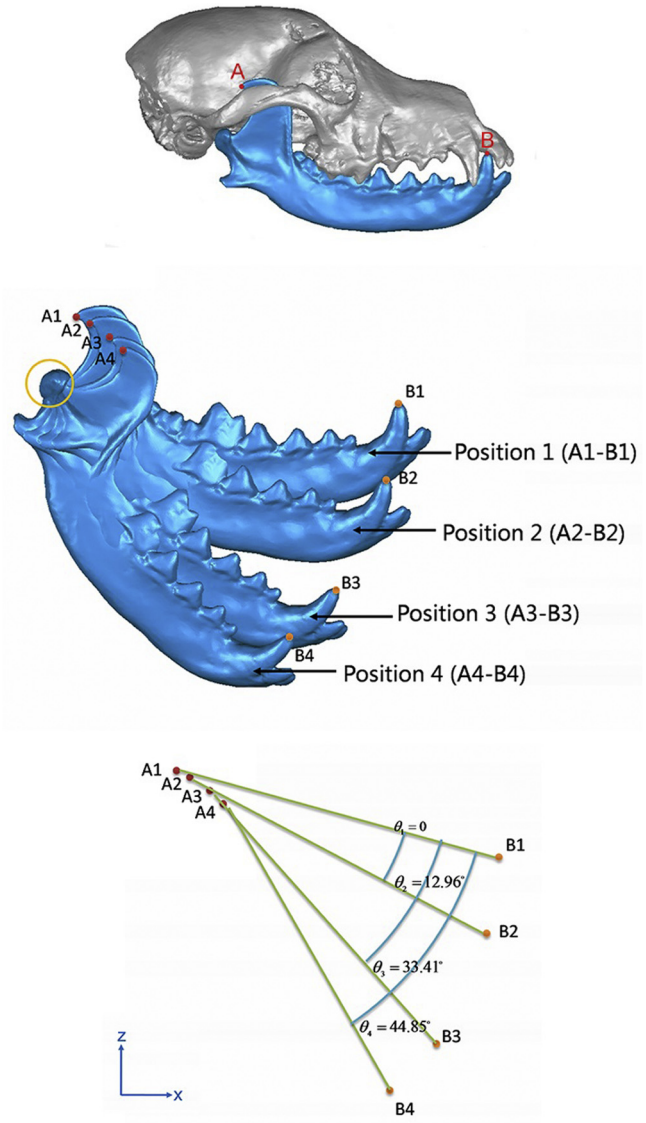

Fig. 3. Four mandible positions (Position 1, fully closed mouth position; Position 2, small mouth-opening position; Position 3, large mouth-opening position; Position 4, maximum mouth-opening position) and the corresponding open angles along the mouth opening trajectory. Points A (coracoid process) and B (canine tooth) are the two markers along the mouth opening trajectory.

The combined fixation structures for the condyle component contained an inlay rod and an onlay plate to strengthen the connection between the prosthesis and the remaining mandible. The inlay rod (a round tapered bar 3 mm in length, with a maximum diameter of 1.6 mm and a 10-degree taper angle around) located on the medial underside of the condyle component was introduced into the intramedullary mandible, with at least 1 mm of bone surrounding the inlay rod. The onlay plate, 4 mm in width, 1 cm in length and an invariable thickness of 1 mm, was designed with a custom-made inner surface to fit the outer surface of the ramus. The bone-contact side of the onlay plate was designed as based on the dimensions of the outer surface of the mandibular ramus to yield a precise fit. Three screw holes on the onlay plate were positioned away from vital structures and into the most appropriate bone for fixation, as had been performed in an earlier study [30]. Screws of maximum possible length were chosen according to the bone thickness at the respective screw position, as determined via the three-dimensional reconstructed geometry model. The screws should be completely embedded within the bone.

In this study, a novel tetrahedral structural design of the open-porous titanium scaffold was proposed and investigated to fabricate the middle portion of the condyle component (Fig. 2). Testing models of the tetrahedral structure were created by using ANSYS simulation software with changeable parameters.

Struts were meshed with BEAM188 elements with circular cross sections, additionally, a mesh density of three elements per strut was applied for accuracy [18]. The material for the model was a titanium alloy (Ti-6Al-4 V).

The behaviour of this structure was compared to that of three different structural designs (cubic, diagonal and truncated pyramidal) proposed and studied by Wieding et al. [18]. Under the same conditions, the mechanical properties of the four structural scaffolds were optimized to yield a structural modulus of 12.8 GPa (mean Young's modulus of the cortical bone and cancellous bone of the beagle condyle [31]). For the tetrahedral structure, the side lengths of the testing models were $3c \times 3c \times 3c$, $6c \times 6c \times 24c$ and $6c \times 6c \times 24c$ (where 'c' represents the size of a basic cell) for uniaxial compression, bending and torsion loadings, respectively. According to the formula presented by Wieding et al. [18], the structural compression, bending and shear modulus of the 4 scaffolds were calculated based on the numerical results.

The tetrahedral structure for the open-porous scaffold offered a sufficient balance between rigidity and weight, and was, thus, chosen for use in the design of the condyle component. As a result, with a mean cell size of 2280 μm and strut diameter of 570 μm,

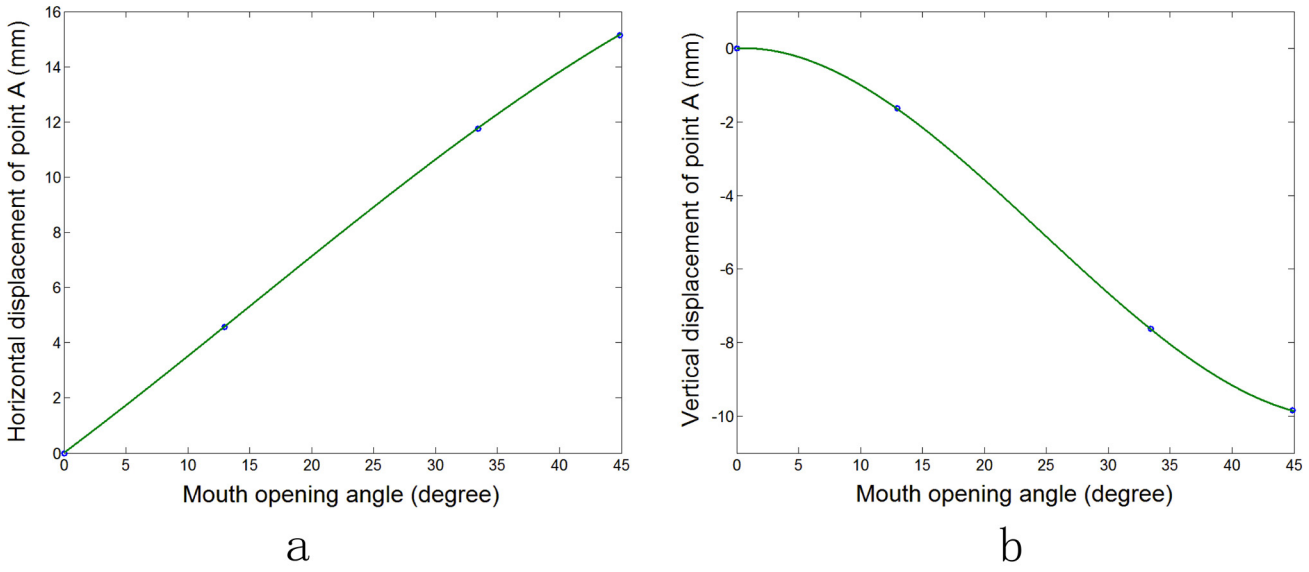

Fig. 4. Kinematics of the mandible. Left panel (a): the relationship curve of the horizontal displacement of Point A and mouth-opening angle; right panel (b): the relationship curve of the vertical displacement of Point A and mouth-opening angle.

the tetrahedral structure yielded a structural modulus of 12.8 GPa. These dimensions and properties were applied to the design of the scaffolds in the condylar component, with the open-porous tetrahedral structure having the same profile as the condyle.

2.2.2. Design of the fossa component

The aim of the designed TMJ prosthesis was to comfortably reproduce the full-range mandible open–close mouth movements of a normal TMJ; thus, the movement behaviour of a healthy TMJ was recorded to facilitate the design of the fossa component. Intact mandible models of four positions observed in the process of mouth opening, i.e. closed, one-third-open, two-thirds-open, and widest open positions, were marked in Points A (coracoid process) and B (canine tooth) for motion analysis (Fig. 3).

The envelope surface of condyle movement was determined via kinematic analysis, with this surface being designed as the lower surface of the fossa component (Figs. 4 and 5); this means that the condyle would be able to move freely along the lower surface of the matched fossa component. The motion of the mandible during mouth opening was simplified to rigid body planar motion along the sagittal plane in this study. Intact mandible models of the four aforementioned mouth-opening positions were generated and aligned in a global coordinate system with the maxilla in the same position. These mandible models were projected onto the sagittal plane and marked in Points A (coracoid process) and B (canine tooth) for motion analysis. The relationship curves between the horizontal/vertical displacement of Point A and the mouth-opening angle were obtained by fitting the coordinates of Point A and the relative angles of Segment AB at the aforementioned four positions with the least-square method. The location of any chosen point on the mandible could be deduced from the relationship curves. As shown in Fig. 4, the horizontal and vertical displacements of Point A (the coracoid process) varied according to the mouth-opening angle, which reflected the kinematics of the mandible. The fabrication process for the envelope surface is illustrated in Fig. 5. First, the dimensional and positional information on the articular surface of the condyle was obtained; then, this information was converted into discrete and dense point clouds. The motion of mouth opening was uniformly decomposed into 11 stages. Based on the kinematics of the mandible, 11 sets of locus points representing 11 condylar positions throughout the movement range of the condyle were calculated and plotted onto a global coordinate system. The envelope points above each of these points generated the envelope point cloud, which consequently formed the envelope surface of the condyle movement. Posterior and anterior stops were incorporated into the design to prevent excessive movement of the mandible.

According to Sinno et al. [3], stability is an important factor in the success of a TMJ reconstruction. The upper surface of the fossa component, which was also considered as the contact interface, was based on skull geometry, locating a best-fit position in the bone (Fig. 6). The space between the envelope surface and the contact interface was the space precisely occupied by the fossa component. Four screw holes were added to the outer plate away from vital structures and into the best possible bone for fixation between the fossa component and the zygomatic arch, as had been done with the condyle component (Fig. 7). Screws of the greatest possible length were chosen; these screws should be completely embedded into the bone.

2.3. Finite element model

The FEA method is an effective tool to demonstrate the biomechanical properties of complex structures [33,34]. The finite element model presented in this study was calculated using ANSYS software. The teeth were considered to yield only marginal influence on the biomechanics of the mandible, particularly with regard to the behaviour of the condyles [35], so were thus removed in our model, as in previous studies [2,36]. For simplicity, only the portion of the skull connecting the fossa component and right zygomatic arch was modelled.

The material properties of the models were assigned based on the results of previous studies [2,31,37] and are given in Table 1. All materials used in this model were considered isotropic, homogeneous, and linear elastic materials. The mandible cortical bone was considered to have a Young's modulus of 12.8 GPa and a Poisson coefficient of 0.3 for experimental validation [31]. The Young's modulus and Poisson coefficient of the condyle component and screws were 114 GPa and 0.3, respectively.

The prosthesis was applied to the right side of the mandible (Fig. 7). Seven 2.0-mm-diameter screws were used to fix the prosthesis, with four being used to fix the fossa component and

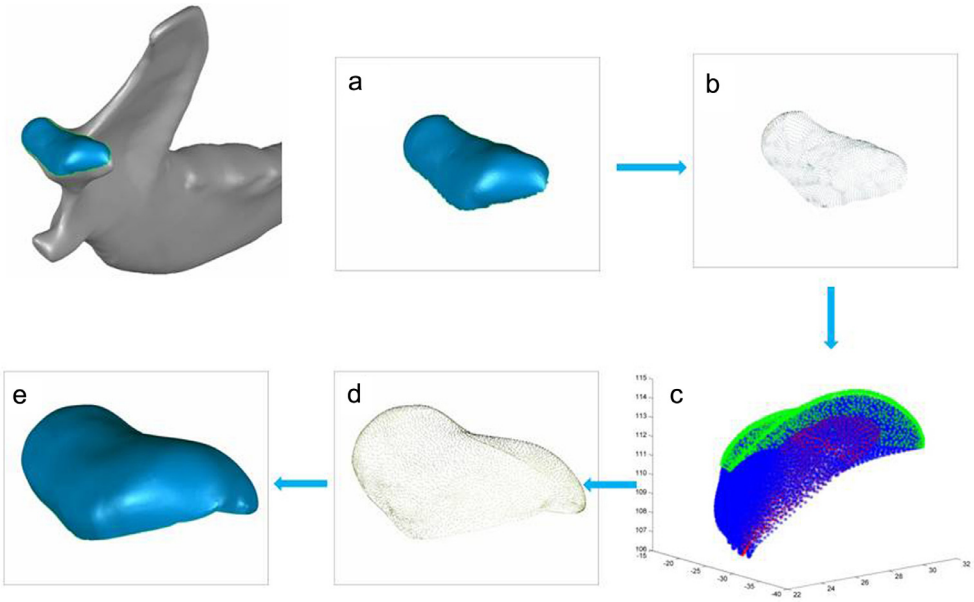

Fig. 5. Creation of the envelope surface of condyle movement. (a) Articular surface of the condyle at the closed position; (b) point clouds of the articular surface of the condyle at the closed position; (c) 11 sets of point clouds of the articular surface throughout the entire movement of the condyle from the closed position (red points) to the widest open position (green points); (d) point clouds of the envelope surface of condyle movement; (e) the envelope surface of condyle movement. (For interpretation of the references to colour in this figure legend, the reader is referred to the web version of this article.)

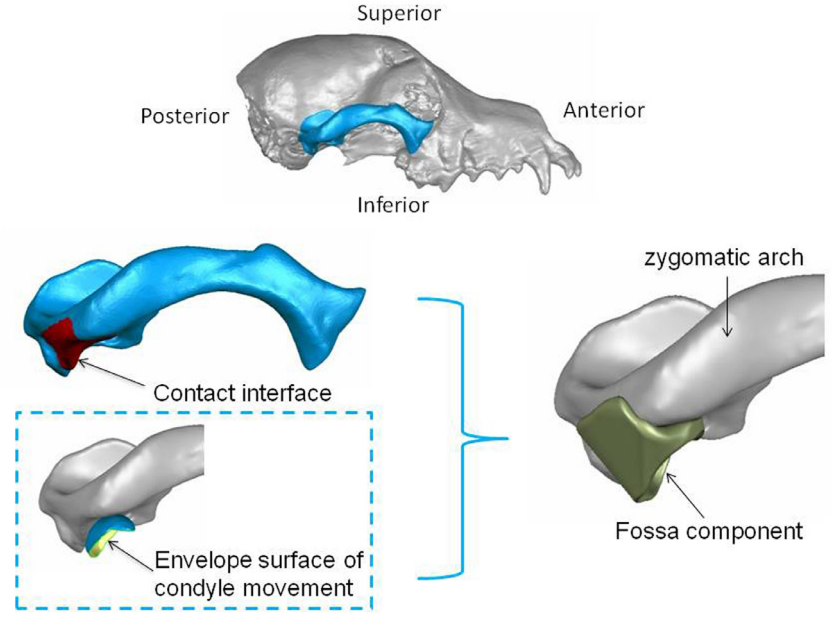

Fig. 6. Fossa component structure and design of the replacement prosthesis. Top panel: right zygoma marked in blue. Lower left panel: the upper surface of the fossa component (contact interface) marked in red, and the lower surface of the fossa component (envelope surface of condyle movement) marked in blue. Lower right panel: the fossa component precisely occupying the space between the contact interface and the envelope surface. (For interpretation of the references to colour in this figure legend, the reader is referred to the web version of this article.)

Table 1
Material properties in the finite element analysis (FEA) model.

Model	Material	Young's modulus (MPa)	Poisson's radio	Tensile strength (MPa)
Skull	Cortical bone	12,800	0.30	
Mandible	Cortical bone	12,800	0.30	
Condyle component	Titanium alloy	114,000	0.30	897
Screws	Titanium alloy	114,000	0.30	897
Fossa component	UHMWPE	500	0.29	

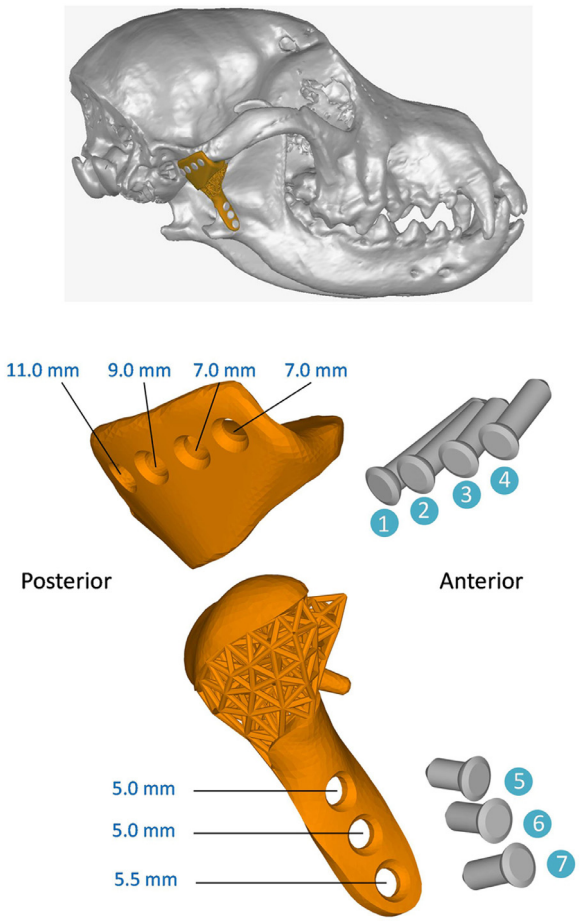

Fig. 7. Assembly diagram of the customized TMJ prosthesis. Top panel: full view of the prosthesis assembled on the skull and the mandible; middle panel: the fossa component with four screws; lower panel: the condyle component with three screws.

three being used to fix the condyle component. Depending on the anatomical structure, screw lengths varying from 5 mm to 11 mm were able to yield adequate fixation. The screws were modelled with pin geometry for simplicity. The screws–prosthesis and screws–bone contact interfaces were considered as bonded. Prosthesis–bone interfaces were modelled as surface-to-surface contact elements with a friction coefficient of 0.3, as based on previously published studies [2,38]. This type of contact seemed to be important when considering the effects of external fixation on load transfer. Between the interface of the fossa component and the condyle component, the friction ratio was considered 0.01.

Rigid-body displacement of the mandible during biting was prevented by the top surfaces of the skull, the left condyle, and the ends of the zygomatic arch, which were fully constrained in all directions. The bone adjacent to the incisor tooth was also constrained in all directions, as shown in Fig. 8. Loads were applied to both sides of the mandible via corresponding muscle forces, which were simulated by distributing groups of parallel vectors across the areas of attachment. The four most important muscles, i.e. the superficial masseter, deep masseter, anterior temporalis, and posterior temporalis, were simulated. All data relevant to the muscle forces were taken from studies by Hu et al. [39]. The location of the muscular area and the direction of muscle forces were defined according to anatomical data.

The bone, implant, and screws were meshed with four-node linear tetrahedral elements, as these elements are well suited to reproduce the irregular and complex geometries. The scaffolds were meshed with circular-section beam elements; a mesh density of three elements per strut was applied. The mesh of the mandible model with the prosthesis, shown in Fig. 8a, consisted of 260,921 elements and 55,618 nodes, whereas the mesh of the intact mandible model, shown in Fig. 8b, consisted of 83,573 elements and 17,914 nodes. They both yielded sufficient density to satisfy the requirements of convergence of the numerical results.

In this study, after the muscle forces were applied in the FEA models, the biomechanical properties of the custom-made TMJ prosthesis were investigated, and the behaviours of an intact mandible and the mandible with the prosthesis were compared. To analyse the strain on the external surface of the mandible, a control line was chosen based on the previous studies [2,10,38]; this line traversed characteristic features present on the external surface of the mandible, including the neck, ramus, angle, and body of the mandible.

3. Results

3.1. Open-porous scaffolds for the condyle component

In order to obtain comparable results, the four structural designs were assumed to have the same structural modulus of 12.8 GPa under uniaxial compression testing [36]. Under bending, the tetrahedral, cubic, diagonal and truncated pyramidal designs exhibited comparable bending modulus values of 10.71 GPa, 7.69 GPa, 12.72 GPa and 10.96 GPa, respectively (Table 2); however, their results under torsional loading were significantly different. The shear modulus of the cubic and truncated pyramidal designs was very low at 0.39 GPa and 0.72 GPa, respectively. The tetrahedral design exhibited a moderately higher shear modulus of 3.29 GPa. Furthermore, the porosities of the four designs varied: 55.40% (tetrahedral), 73.12% (cubic), 44.23% (diagonal) and 72.37% (truncated pyramidal).

3.2. TMJ prosthesis assembly behaviour

The von Mises stress in the fossa component is illustrated in Fig. 9a. The magnitudes of stress were small, less than 10 MPa, with the exception of the critical region. The critical regions in the fossa component, particularly about Screw 4, were observed to be anteriorly and laterally located, indicating that these regions were the main load-transfer regions in the TMJ prosthesis (Fig. 9c).

Fig. 9b shows the von Mises stress in the condyle component. Critical regions could be observed in the lateral areas of the scaffolds, with stress values exceeding 100 MPa. Without consideration of the scaffolds, the anterior and lateral areas of the articular surface and regions near the inlay rod and screw holes in the onlay plate also exhibited relatively high stress distributions. Regarding the screws used to fix the condyle component, the critical region was observed about Screw 5, with the peak von Mises stress being 55.09 MPa (Fig. 9d). In general, the highest peak stress value in the condyle component was far below the ultimate tensile strength of the titanium alloy (897 MPa) [40].

3.3. Bone behaviour

The maximum principal and minimum principal strains along the control line on the external surface of the mandible are shown in Fig. 10, respectively. The maximum principal strain increased by less than two times the initial value, while the minimum principal strain reduced to one-third the initial value after the prosthesis was applied; these results showed the influence of the prosthesis on the right condyle. The results also demonstrated that the prosthesis negligibly influenced the strain on the opposite condyle.

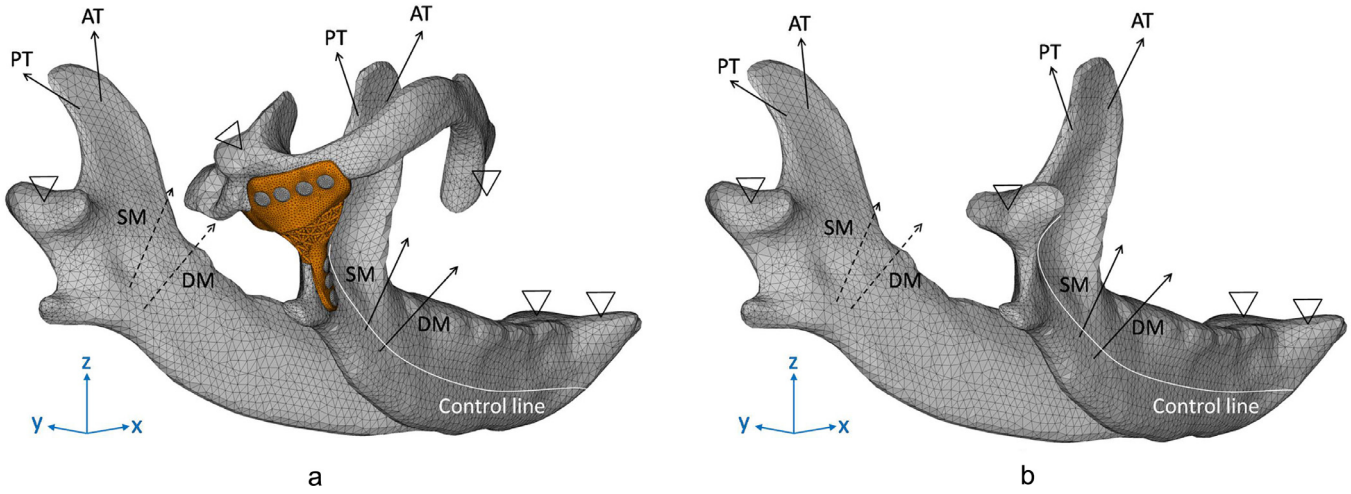

Fig. 8. Finite element model, boundary conditions, and muscular actions. Left panel (a): mandible with the prosthesis, and right panel (b): intact mandible. DM, deep masseter; SM, superficial masseter; AT, anterior temporal; PT, posterior temporal. The control lines are in white.

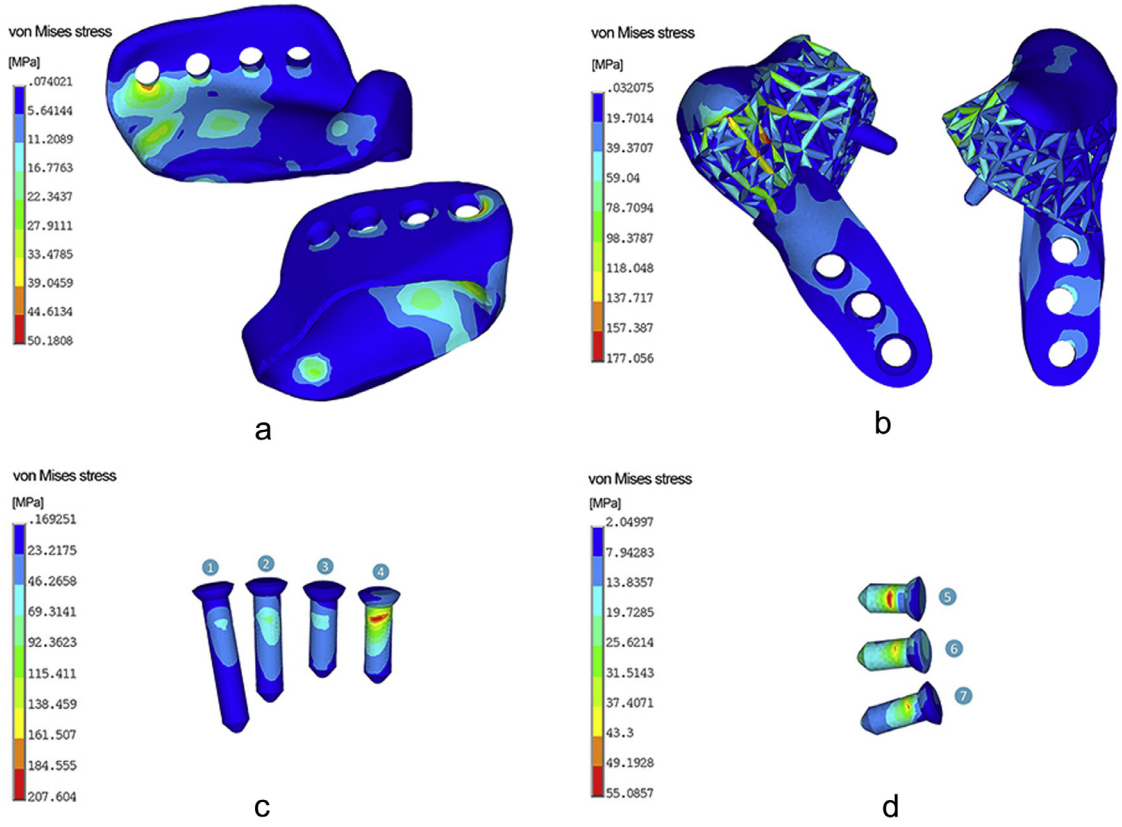

Fig. 9. von Mises stress (MPa) on (a) the fossa component, (b) the condyle prosthesis, (c) each screw used to fix the fossa prosthesis, and (d) each screw used to fix the condyle prosthesis.

Fig. 11 illustrates that the maximum and minimum principal strain distributions in the right condyle neck were affected by the TMJ prosthesis. In the intact condyle, the critical region was observed in the condyle neck. When the mandible was implanted with the TMJ prosthesis, the magnitude of the compressive strain on the condyle neck was lower than that in the intact mandible, with the exception of the area about the screws; additionally, the magnitude of the strain at the scaffold–bone interface was relatively high. The fixation of the prosthesis is a critical factor for TMJ implant success [32]. The bone near Screw 5 exhibited a high degree of minimum principal strain, peaking at approximately around 2100 $\mu\varepsilon$, and the remaining two screws, Screws 6 and 7, did not facilitate much load transfer between the prosthesis and bone.

Observation of the results on the right zygomatic arch revealed that the screw fixation regions of the fossa component became critical positions of the skull (Fig. 12). High tension and compressive strains were observed near the inlet of Screws 4 and 3, where they reached values of 3452 $\mu\varepsilon$ and 3961 $\mu\varepsilon$, respectively; however, these values were lower than the critical value (4000 $\mu\varepsilon$) that is considered to cause hypertrophy of bone [41].

Table 2
Geometrical values of the design parameters and mechanical results for the four designs investigated (tetrahedral, cubic, diagonal and truncated pyramidal).

Parameter	Design	Tetrahedral	Cubic	Diagonal	Truncated pyramidal
Geometrical	Strut diameter (μm)	570[d]	600[d]	631[d]	615[d]
	Size of basic cell (μm)	2280[c]	1910[c]	1900[c]	2000[c] 998[a] 3869[h]
	Porosity (%)	55.40	73.12	44.23	72.37
Mechanical	Structure modulus (GPa)	12.80	12.80	12.80	12.80
	Bending modulus (GPa)	10.71	7.69	12.72	10.96
	Shear modulus (GPa)	3.29	0.39	8.58	0.72

[d] strut diameter
[c] size of the basic cell
[a] length of the additional connection strut in truncated pyramidal structure
[h] height of the basic cell in truncated pyramidal structure

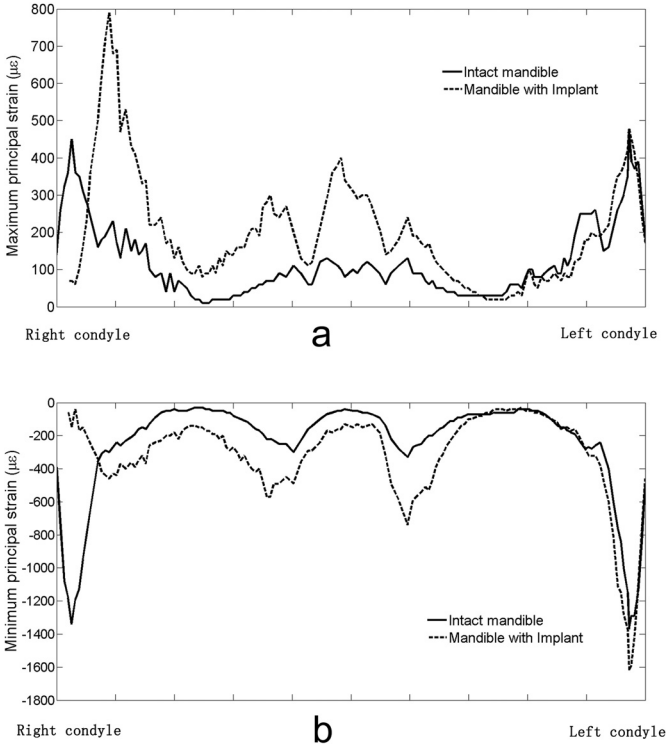

Fig. 10. (a) Maximum principal strain ($\mu\varepsilon$) and (b) minimum principal strain ($\mu\varepsilon$) on the external surface of the mandible along the control line (right condyle to left condyle).

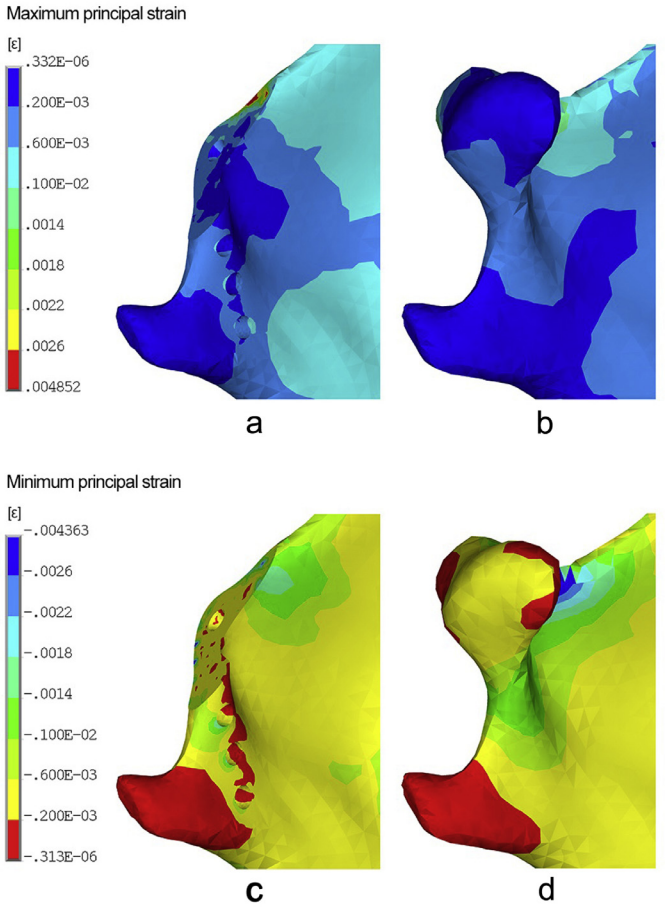

Fig. 11. Maximum principal strain (ε) on the right condyle of the mandible: (a) for the mandible with the prosthesis, and (b) for an intact mandible; minimum principal strain (ε) on the right condyle of the mandible: (c) for the mandible with the prosthesis, and (d) for an intact mandible.

4. Discussion

A novel individually designed 3D printing custom-made alloplastic TMJ prosthesis was developed in this study. The custom-made profile was proven adaptable to individual anatomical structures, and the tetrahedral scaffold was optimized to reduce the stress shielding effect in the alloplastic condyle. An inlay rod and an onlay plate in the base of the prosthesis were also designed to strengthen the connection with the remaining portion of the mandible. UHMWPE has had long-term success as a joint spacer in hip and knee replacements [42]. Thus, it was also used to construct the fossa in our design.

Some researchers have noted that the design of TMJ alloplastic replacements should emphasize engineering improvements in material selection, modulus, stiffness, notch sensitivity, and modularity [3]. In this study, the prosthesis was designed to be made of Ti-6Al-4 V, a highly biocompatible material. The additive manufactured trabecula in the artificial condyle was effectively able to promote high porosity in the prosthesis, thereby reducing its stiffness. The trabecula architecture within the condyle was also completely optimized to closely match the Young's modulus of bone, which consequently reduced the stress shielding effect. The connection structure for the inlay rod and onlay plate was also designed to reinforce the connection between the prosthesis and the remaining mandible. Furthermore, the advantage of additive manufacturing is that various components with varying functions can be concurrently fabricated, with finer details being adjustable to satisfy a variety of engineering requirement. SLM 3D printing

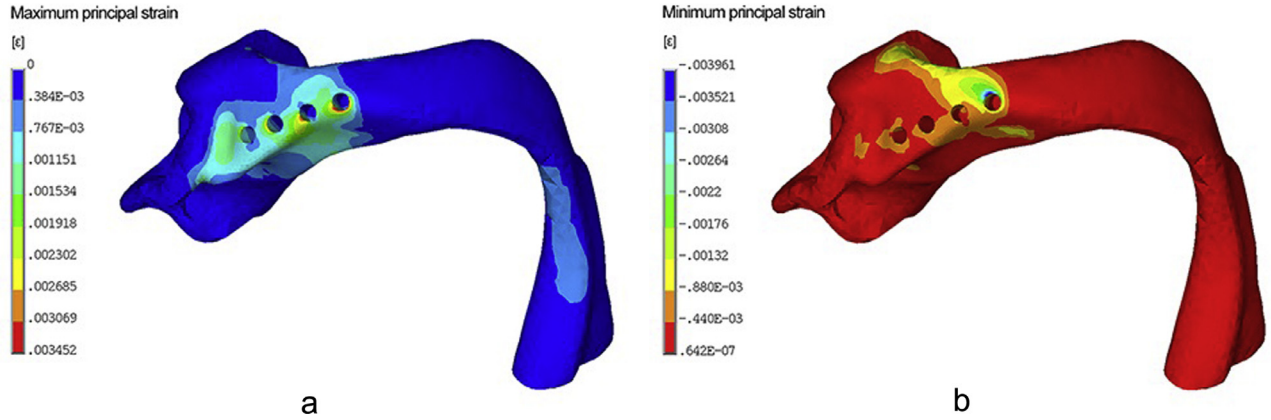

Fig. 12. (a) Maximum and (b) minimum principal strains (ε) on the skull.

technology can be used to construct irregular shapes and make complex parts/designs a reality. The purpose of optimizing scaffold fabrication is to overcome biological constraints and to minimize the stress shielding effect and weight of the prosthesis.

Based on Wolff's law, the trabecular arrangement in bone affords an adaptable reaction to the loads under which it is placed [43]. Therefore, making the scaffolds by considering load transfer may be the optimal way to fabricate bone substitution materials, such as Ti-6Al-4 V.

In this study, four different trabecular designs (tetrahedral, cubic, diagonal and truncated pyramidal) were compared. The cubic structure yields the highest porosity, but it exhibits weak bearing capacity against bending and especially against torsion. The diagonal design offers the highest rigidity against bending and particularly against torsion, among these four designs. However, it yields increased weight with low porosity. The truncated pyramidal design offers high bending-bearing capacity and high porosity, but it exhibits weak torsion-bearing capacity. The tetrahedral design yields relatively high porosity, a relatively high bending modulus, and a relatively high shear modulus, which proved to be a good balance between rigidity and weight. Thus, this type of design was chosen in this study.

In the current condyle component, some vertical struts that connected the articular surface of the condyle component and onlay plate suffered a high level of stress (Fig. 9b). This appears to be a clear indication of load-transfer, as it coincided with the arrangement order of the trabecular bone structure.

Though all of the US Food and Drug Administration (FDA)-approved alloplastic TMJ implants use an onlay connection to fix the prosthesis, several authors have proposed that buccal-fixed plates could withstand undesirable forces that could lead to fracturing of the plates [44–46]. In this study, the connection between the prosthesis and the remaining bone tissue comprised of two structures: an inlay rod and an onlay plate, to ensure the long-term stability of the prosthesis.

In addition to the popular applications of endoprostheses to replace hip and knee joints, there have also been several studies that have used endoprostheses to restore mandibular defects [34,46–48]. These prostheses are designed to restore large mandibular defects, such as those of the mandibular body and ramus.

Goh et al. evaluated the feasibility of replacing the condyle and ascending ramus with an endoprostheses in the Macaca fascicularis [47]. They fixed the modular endoprosthesis with polymethylmethacrylate (PMMA) cement. Although the results showed that two out of eight monkeys sustained fistulas with linear radiolucency, which further indicated chronic infection at the cement–bone interface, modular endoprostheses for the replacement of the condyle and ramus unit were feasible for the restoration of normal TMJ function.

Ramos et al. employed FEA to assess the strain distribution of an intramedullary condyle component and concluded that intramedullary fixation improved strain distribution [38]. The intramedullary fixation yielded behaviour that was more similar to the intact mandible than that of fixation via an external connection with surgical screws. Their research helped us to design a TMJ prosthesis with an inlay rod. The mandibular condyle neck is thin, however, so it can only fit a thin inlay rod. Therefore, an onlay plate fixed to the outer surface of the ramus was also designed to strengthen the connection between the prosthesis and the remaining mandibular ramus; this method is in line with the methods of current commercial alloplastic TMJs in use.

TMJ replacement loading has previously been compared via FEA for standard and custom-made temporal components [9]. In that study, the authors uniformly thickened the temporal fossa surface to construct the custom-made temporal component. In our study, the TMJ fossa was custom-made not only based on the geometry of the temporal articular surface, but also with regard to the trajectory of movement of the condyle. Four condyle positions, as described above, were calculated by using ANSYS software to establish the trajectory of the condyle. The articular surface of the condyle travelled along this trajectory to form the lower surface of the TMJ fossa.

Regarding the fossa component, the stress at the critical region was relatively high at nearly 50 MPa, which is indicative of the possibility of abrasion of the implant with long-term use. Regarding fixation of the fossa component, the critical region was observed about Screw 4 (Fig. 9c). In this region, the peak von Mises stress was 207.6 MPa. The von Mises stress at the end of Screw 1 was lower than 23 MPa, which indicated that Screw 1 could be shortened to some extent while still maintaining stability.

Overall, the strain distribution results were relatively symmetrical for the intact mandible; additionally, the magnitudes of the strains in the two condyles were much higher than that in the frontal region. The TMJ prosthesis altered the strain distributions on the surface of the mandible relative to those on the surface of the intact mandible; this led to non-symmetrical mechanical behaviour along the control line. The prosthesis yielded significant effects on the right condyle, which is where the prosthesis was implanted; these effects included increasing the maximum principal stress between 0.5 and 2.5 times the initial value and altering the minimum principal stress. In addition, the prosthesis increased the strain in the frontal region of the mandible and yielded marginal effects on the opposite side of the mandible.

When the mandible was implanted with a TMJ prosthesis, the magnitude of the compressive strain on the condyle neck was lower than that in the intact mandible, with the exception being the area surrounding the screws, and the magnitude of the strain on the scaffold–bone interface was relatively high; this implied that a large part of the load was transferred via the inlay rod and scaffold–bone interface. This result indicated that the inlay rod and the scaffold–bone interface primarily supported the prosthesis, which, thus, facilitated the osseointegration and long-term stability of the prosthesis.

In conclusion, the results showed that the custom-made TMJ prosthesis yielded good load-transfer properties and that the appropriate strain distribution pattern on the bone provided a suitable environment for bone adaptation and integration, two benefits that lower the failure risk of screw fixation. This novel, custom-made alloplastic TMJ prosthesis using SLM could be a suitable option for TMJ replacement. A future in vivo study using this prosthesis would further prove its effectiveness.

Ethical approval

The protocol of this study was approved by the Peking University Institutional Review Board (LA2014244). The guidelines for the care and use of laboratory animals of the Ministry of Science and Technology of the People's Republic of China were observed.

Conflict of interest

The authors confirm that there is no conflict of interest in relation to this work.

Acknowledgment

This work was supported by the Peking University Academy for Advanced Interdisciplinary Studies (grant number 2014-4-1).

Supplementary materials

Supplementary material associated with this article can be found, in the online version, at doi:10.1016/j.medengphy.2017.04.012.

References

[1] Vega LG, Gonzalez-Garcia R, Louis PJ. Reconstruction of acquired temporomandibular joint defects. Oral Maxillofac Surg Clin North Am 2013;25:251–69.
[2] Ramos A, Mesnard M. Christensen vs Biomet microfixation alloplastic TMJ implant: are there improvements? A numerical study. J Craniomaxillofac Surg 2015;43:1398–403.
[3] Sinno H, Tahiri Y, Gilardino M, Bobyn D. Engineering alloplastic temporomandibular joint replacements. Mcgill J Med 2011;13:63–70.
[4] Kashi A, Chowdhury AR, Saha S. Finite element analysis of a TMJ implant. J Dent Res 2010;89:241–5.
[5] Kent JN. An important lesson about biomaterials in the TMJ. J Oral Maxillofac Surg 1991;49:442–3.
[6] Koolstra JH. Biomechanical analysis of the influence of friction in jaw joint disorders. Osteoarthritis Cartilage 2012;20:43–8.
[7] Tanaka E, Koolstra JH. Biomechanics of the temporomandibular joint. J Dent Res 2008;87:989–91.
[8] Mercuri LG. Alloplastic temporomandibular joint replacement: rationale for the use of custom devices. Int J Oral Maxillofac Surg 2012;41:1033–40.
[9] Ramos A, Mesnard M. Comparison of load transfers in TMJ replacement using a standard and a custom-made temporal component. J Craniomaxillofac Surg 2014;42:1766–72.
[10] Ramos A, Mesnard M. The stock alloplastic temporomandibular joint implant can influence the behavior of the opposite native joint: a numerical study. J Craniomaxillofac Surg 2015;43:1384–91.
[11] Wolford LM, Dingwerth DJ, Talwar RM, Pitta MC. Comparison of 2 temporomandibular joint total joint prosthesis systems. J Oral Maxillofac Surg 2003;61:685–90.
[12] Leandro LF, Ono HY, Loureiro CC, Marinho K, Guevara HA. A ten-year experience and follow-up of three hundred patients fitted with the Biomet/Lorenz microfixation TMJ replacement system. Int J Oral Maxillofac Surg 2013;42:1007–13.
[13] Leiggener CS, Erni S, Gallo LM. Novel approach to the study of jaw kinematics in an alloplastic TMJ reconstruction. Int J Oral Maxillofac Surg 2012;41:1041–5.
[14] Huiskes R, Weinans H, van Rietbergen B. The relationship between stress shielding and bone resorption around total hip stems and the effects of flexible materials. Clin Orthop Relat Res 1992;274:124–34.
[15] Piao C, Wu D, Luo M, Ma H. Stress shielding effects of two prosthetic groups after total hip joint simulation replacement. J Orthop Surg Res 2014;9:71–8.
[16] Warnke PH, Douglas T, Wollny P, Sherry E, Steiner M, Galonska S, et al. Rapid prototyping: porous titanium alloy scaffolds produced by selective laser melting for bone tissue engineering. Tissue Eng Part C Methods 2009;15:115–24.
[17] Ponader S, von Wilmowsky C, Widenmayer M, Lutz R, Heinl P, Korner C, et al. In vivo performance of selective electron beam-melted Ti-6Al-4 V structures. J Biomed Mater Res A 2010;92:56–62.
[18] Wieding J, Wolf A, Bader R. Numerical optimization of open-porous bone scaffold structures to match the elastic properties of human cortical bone. J Mech Behav Biomed Mater 2014;37:56–68.
[19] Taniguchi N, Fujibayashi S, Takemoto M, Sasaki K, Otsuki B, Nakamura T, et al. Effect of pore size on bone ingrowth into porous titanium implants fabricated by additive manufacturing: an in vivo experiment. Mater Sci Eng C Mater Biol Appl 2016;59:690–701.
[20] Chen J, Luo C, Zhang C, Zhang G, Qiu W, Zhang Z. Design and fabrication of the custom-made titanium condyle by selective laser melting technology. Zhonghua Kouqiang Yixue Zazhi 2014;49:625–30.
[21] Evans HE, Lahunta AD. Miller's anatomy of the dog. 4th ed. Missouri: Elsevier; 2013.
[22] Verstraete FJM, Lommer MJ, Bezuidenhout AJ. Oral and maxillofacial surgery in dogs and cats. New York: Elsevier; 2012.
[23] Brown BN, Chung WL, Pavlick M, Reppas S, Ochs MW, Russell AJ, et al. Extracellular matrix as an inductive template for temporomandibular joint meniscus reconstruction: a pilot study. J Oral Maxillofac Surg 2011;69:e488–505.
[24] Miyamoto H, Shigematsu H, Suzuki S, Sakashita H. Regeneration of mandibular condyle following unilateral condylectomy in canines. J Craniomaxillofac Surg 2004;32:296–302.
[25] Del PA, Doblare M. 3D finite element simulation of the opening movement of the mandible in healthy and pathologic situations. J Biomech Eng 2006;128:242–9.
[26] Kashi A, Chowdhury AR, Saha S. Finite element analysis of a TMJ implant. J Dent Res 2010;89:241–5.
[27] Perez DPA, Doblare M. Finite element analysis of the temporomandibular joint during lateral excursions of the mandible. J Biomech 2006;39:2153–63.
[28] Tanaka E, Del PR, Tanaka M, Asai D, Hirose M, Iwabe T, et al. Three--dimensional finite element analysis of human temporomandibular joint with and without disc displacement during jaw opening. Med Eng Phys 2004;26:503–11.
[29] Maurer P, Holweg S, Schubert J. Finite-element-analysis of different screw-diameters in the sagittal split osteotomy of the mandible. J Craniomaxillofac Surg 1999;27:365–72.
[30] Haq J, Patel N, Weimer K, Matthews NS. Single stage treatment of ankylosis of the temporomandibular joint using patient-specific total joint replacement and virtual surgical planning. Br J Oral Maxillofac Surg 2014;52:350–5.
[31] Kawahara H, Kawahara D, Hayakawa M, Tamai Y, Kuremoto T, Matsuda S. Osseointegration under immediate loading: biomechanical stress-strain and bone formation–resorption. Implant Dent 2003;12:61–8.
[32] Mercuri LG. Temporomandibular joint reconstruction. Alpha Omegan 2009;102:51–4.
[33] Hsu JT, Huang HL, Tsai MT, Fuh LJ, Tu MG. Effect of screw fixation on temporomandibular joint condylar prosthesis. J Oral Maxillofac Surg 2011;69:1320–8.
[34] Wong RC, Tideman H, Merkx MA, Jansen J, Goh SM. The modular endoprosthesis for mandibular body replacement. Part 2: finite element analysis of endoprosthesis reconstruction of the mandible. J Craniomaxillofac Surg 2012;40:e487–97.
[35] Korioth TW, Romilly DP, Hannam AG. Three-dimensional finite element stress analysis of the dentate human mandible. Am J Phys Anthropol 1992;88:69–96.
[36] Conci RA, Tomazi FH, Noritomi PY, Da SJ, Fritscher GG, Heitz C. Comparison of neck screw and conventional fixation techniques in mandibular condyle fractures using 3-dimensional finite element analysis. J Oral Maxillofac Surg 2015;73:1321–7.
[37] Ashman RB, Rosinia G, Cowin SC, Fontenot MG, Rice JC. The bone tissue of the canine mandible is elastically isotropic. J Biomech 1985;18:717–21.
[38] Ramos A, Mesnard M, Relvas C, Completo A, Simoes JA. Theoretical assessment of an intramedullary condylar component versus screw fixation for the condylar component of a hemiarthroplasty alloplastic TMJ replacement system. J Craniomaxillofac Surg 2014;42:169–74.
[39] Hu K, Zhou J, Liu H, Hu M, Wang D, Rong Q, et al. Development of the three--dimensional finite element model of adult dog temporomandibular joint in functional loading. Acad J PL A Postgrad Med Sch; 1997. p. 167–9.
[40] Li P, Shen L, Li J, Liang R, Tian W, Tang W. Optimal design of an individual endoprosthesis for the reconstruction of extensive mandibular defects with finite element analysis. J Craniomaxillofac Surg 2014;42:73–8.
[41] Roberts W, Huja S, Roberts J. Bone modelling: biomechanics, molecular mechanisms and clinical perspectives. Semin Orthod 2004;10:123–61.
[42] Galvin A, Brockett C, Williams S, Hatto P, Burton A, Isaac G, et al. Comparison of wear of ultra-high molecular weight polyethylene acetabular cups against surface-engineered femoral heads. Proc Inst Mech Eng H 2008;222:1073–80.
[43] Frost HM. Skeletal structural adaptations to mechanical usage (SATMU): 1. Redefining Wolff's law: the bone modeling problem. Anat Rec 1990;226:403–13.

[44] Spencer KR, Sizeland A, Taylor GI, Wiesenfeld D. The use of titanium mandibular reconstruction plates in patients with oral cancer. Int J Oral Maxillofac Surg 1999;28:288–90.
[45] Shibahara T, Noma H, Furuya Y, Takaki R. Fracture of mandibular reconstruction plates used after tumor resection. J Oral Maxillofac Surg 2002;60:182–5.
[46] Pinheiro M, Alves JL. The feasibility of a custom-made endoprosthesis in mandibular reconstruction: Implant design and finite element analysis. J Craniomaxillofac Surg 2015;43:2116–28.
[47] Goh BT, Lee S, Tideman H, Jansen JA, Stoelinga PJ. Replacement of the condyle and ascending ramus by a modular endoprosthesis in Macaca fascicularis—part 4: evaluation of the temporomandibular joints. J Oral Maxillofac Surg 2010;68:2136–45.
[48] Wong RC, Tideman H, Merkx MA, Jansen J, Goh SM. The modular endoprosthesis for mandibular body replacement. Part 1: mechanical testing of the reconstruction. J Craniomaxillofac Surg 2012;40:e479–86.